GEOPHYSICS, VOL. 68, NO. 1 (JANUARY-FEBRUARY 2003); P. 274–285, 10 FIGS.
10.1190/1.1543213

Crooked-line 2D seismic reflection imaging in crystalline terrains: Part 1, data processing

Mladen R. Nedimović* and Gordon F. West‡

ABSTRACT

For cost and access reasons, most of the seismic reflection data collected in crystalline terrains have been acquired by 2D crooked-line profiling. When the survey geometry is significantly irregular and the geologic structures have cross-profile dip, several standard 2D imaging procedures severely underperform. As a result, reflection signal is poorly aligned across individual common midpoint (CMP) gathers, and much is lost during the CMP stack. To improve imaging, either the methods used to align signal before stack need to be modified or more tolerant methods of combining trace signals than the standard CMP stack need to be applied.

Because a high-fold 2D crooked-line profile is really a 3D survey of a swath of terrain around the processing line, better signal alignment before CMP stacking may be achieved by revisiting the traveltime equation and including the cross-dip terms into the moveout calculations. Therefore, in addition to the correction of NMO and in-line dip moveout (DMO), we also locally compute and subsequently remove cross-dip moveout (CDMO). This requires a procedure for estimating the amount of cross-dip associated with each local reflection event. Stacking after the successful removal of the CDMO yields what we call an optimum cross-dip stack—a seismic section that is significantly more complete and informative than the standard stack. Alternatively, amplitude stacking appears to be more robust to residual time anomalies. When little or no cross-dip information can be extracted from the 2D crooked-line data, we use it as a last resort to obtain a section that contains more structural information than the standard stack.

INTRODUCTION

Elastic interfaces in crystalline igneous and metamorphic rocks have complicated shape, orientation, and dip. To image structures correctly, a 3D seismic reflection survey method ought to be used. But because of the inaccessibility of most crystalline terrains and the high cost of 3D seismic reflection investigations, most data collection has been carried out by 2D profiling on local roads. Since the roads typically wind through rough countryside, the seismic acquisition lines are crooked, which further complicates imaging. To improve image quality, crooked-line profiling is often done at a very high density, and the average CMP fold generally exceeds a hundred data traces per gather.

Considerable success has been achieved by high-fold 2D crooked-line imaging in crystalline terrains, especially at crustal scale, and many structures have been mapped at least in a general way. In spite of that, routine data-quality checks indicate that significant loss of recorded reflectivity occurs during standard data processing. Much more reflection signal appears to be present in shot gathers than in the final stack.

We have used both field and synthetic data to investigate this phenomenon. Our study shows that the loss of reflection signal occurs during standard stacking and results from poor alignment of reflection events in CMP gathers. We also find that better signal alignment before stacking may be achieved by accounting for the 3D character of the 2D crooked-line data. This is done by using an NMO equation that incorporates the cross-dip moveout (CDMO) term into the reflection traveltime calculation. The final products are a much improved stack and cross-dip information. When the CDMO analysis fails, we find it useful to combine trace absolute amplitudes.

Presented at the 69th Annual Meeting, Society of Exploration Geophysicists. Manuscript received by the Editor February 27, 2001; revised manuscript received April 18, 2002.
*Formerly Geological Survey of Canada—Pacific, Natural Resources Canada; presently Columbia University, Lamont-Doherty Earth Observatory, 61 Route 9W, P.O. Box 1000, Palisades, New York 10964-8000. E-mail: mladen@ldeo.columbia.edu.
‡University of Toronto, Geophysics Labs, Department of Physics, 60 St. George Street, Toronto, Ontario M5S 1A7, Canada. E-mail: west@physics.utoronto.ca.

Amplitude stack preserves much of the poorly aligned signal and yields sections that are surprisingly informative about large-scale structures. In this paper we describe the suggested solutions for improved stacking on crooked lines and present the obtained results.

The data

Two field data examples are examined in this paper. They were acquired over the exposed Archean crust of the Canadian Superior province and involve typically crooked profiles. The first example is a comparatively high-resolution Sturgeon Lake line (Figure 1a) collected by Noranda Inc. for mining exploration purposes in the Sturgeon Lake greenstone belt of the central Wabigoon subprovince in northwestern Ontario. The second field survey is a Project Lithoprobe crustal scale line 23 (Figure 1b) acquired in the Abitibi greenstone belt of the Abitibi subprovince, also in Ontario. For both data sets the CMP fold obtained is very irregular but is consistently well over one hundred data traces per gather. The irregularity of the CMP fold is not only because of the crookedness of the profiles but is also a result of shot gaps which occurred frequently along the profiles. Specific details of the two field surveys are given in Appendix A.

Synthetic data sets examined and presented in this paper all used the actual geometries of the two field surveys and were computed by using a ray-Born method. Only direct P-waves were considered. For details about modeling, see Appendix B.

Focusing problems

When 2D seismic profiling is carried out on crooked lines, the trace midpoints cover an area surrounding the survey line at a variable density (Figure 2). A crooked-line survey therefore samples a much larger subsurface area than a straight-line survey, which must lead to higher uncertainty about the imaged structures. To make imaging feasible, CMP bin gathers are formed (a) by dividing the midpoint area into bins whose centers are found on the chosen processing line, often called the slalom line, and (b) by collecting the data traces within each CMP bin and associating them with the bin's center point. The processing line can be smooth or comprised of one or more straight segments.

In straight-line processing, we expect reflection events in an NMO-corrected CMP gather to be horizontally aligned to within about a quarter-cycle if static corrections have been made correctly. Some systematic deviation from horizontal may be evident if the velocity analysis is inaccurate or DMO is important. But, as we show in Figure 3, crooked-line survey data often have a different character. Events exhibit correlation with changing offset and from one CMP bin gather to the next. But the alignment of correlation is wavy instead of straight, and the standard CMP stack rejects much of the reflection signal.

Although the data extract shown in Figure 3a (CMP bin 4555, Sturgeon Lake line) is typical in its character, it is for a time range of 2.3 to 2.7 s and for offsets smaller than ±1.75 km. Thus, it is unlikely that varying in-line dip of the reflectors (DMO) is the cause of the apparent wobbly alignment and associated interference between overlapping reflection events. As we shall illustrate on synthetic data, uncorrected CDMO is likely the main cause.

Figure 4 depicts the Sturgeon Lake line geometry with a 30° cross-line dipping layer and part of the CMP bin gather 2915 of the computed synthetic data. Cross-offset spread, the extreme range of midpoint cross-line offset in the gather, is ~470 m. The large residual time anomaly seen in Figure 4c is the result of the CDMO. The extreme magnitude of the CDMO is ~50 ms—about five times larger than the 10-ms dominant period of the Butterworth minimum-phase wavelet used in modeling the Sturgeon Lake line data. In fact, the CDMO in crooked-line data is highly significant even for more moderate reflector dips and gathers with relatively small cross-profile spread.

3D structure, 2D surveying.—In 2D seismic reflection surveying, the desired objective is a vertical cross-section through the geology under the survey line. Theoretically, this can be achieved when the geology has only low dip or exhibits only 2D structure and the survey profile crosses the geological strike. When the geological structure is more complex and when the reflectors dip in a great variety of directions, 2D surveying even on straight lines cannot produce a true structural cross-section. At best, a synthetic zero-offset seismic time (SZOST) section can be produced that approximates a single slice of a hypothetical 3D SZOST volume for the region. We can apply 2D migration to this slice, but even in the best case the resulting structural section is not a 2D section through the geology because reflectors imaged by it may not lie directly under the survey profile. In the cross-profile direction, the migrated data remain an SZOST section; thus, there is a cylindrical ambiguity of all reflector positions about the survey profile.

Because of the scattering of source–receiver midpoints, a 2D crooked-line survey is really a kind of 3D survey of a swath of terrain around the processing line. However, the data are limited in quantity and have an uneven spatial distribution, only a small range of azimuths, and a small aperture in the cross-profile direction. In a companion paper (Nedimović and West, 2003), we study the potential for using 3D prestack migration to position the observed reflection events in space. In this paper we concentrate on trying to obtain the same kind of SZOST section that might be obtained from a straight-line 2D survey, plus we obtain some limited information about the cross-profile dip of reflectors that can help reduce the cylindrical ambiguity of that SZOST section. The problem is therefore largely one of preventing the cross-dip time anomalies evident in the crooked-line survey data from damaging the CMP stack. The reward is the obtained 3D structural information.

Traveltime equation.—For data collected on straight lines, the CMP traveltime equation is

$$t^2(x, h) = t_0^2(x) + p^2h^2, \tag{1}$$

where x is the position of the CMP on the survey profile, h is the source–receiver offset, $t(x, h)$ is the source–receiver traveltime via the reflection point, $t_0(x)$ is the zero-offset reflection traveltime, and p is an unknown slowness parameter that depends on the host medium velocity and the reflector geometry. In the case of mild reflector dip and only mild heterogeneity of host medium velocity, $p = 1/V_{\text{rms}}$, where V_{rms} is the root mean square velocity of the host medium.

It is not hard to generalize equation (1) for the case of crooked survey lines, as is given in Appendix C:

$$t^2(x, y, h) = (t_0(x) + p_y y)^2 + p^2 h^2. \qquad (2)$$

In this, x is the position of the CMP bin center on the processing line; y is the cross-line offset, the shortest distance from the midpoint to the processing line; and p and p_y are wave slownesses associated with the given host medium velocity and the

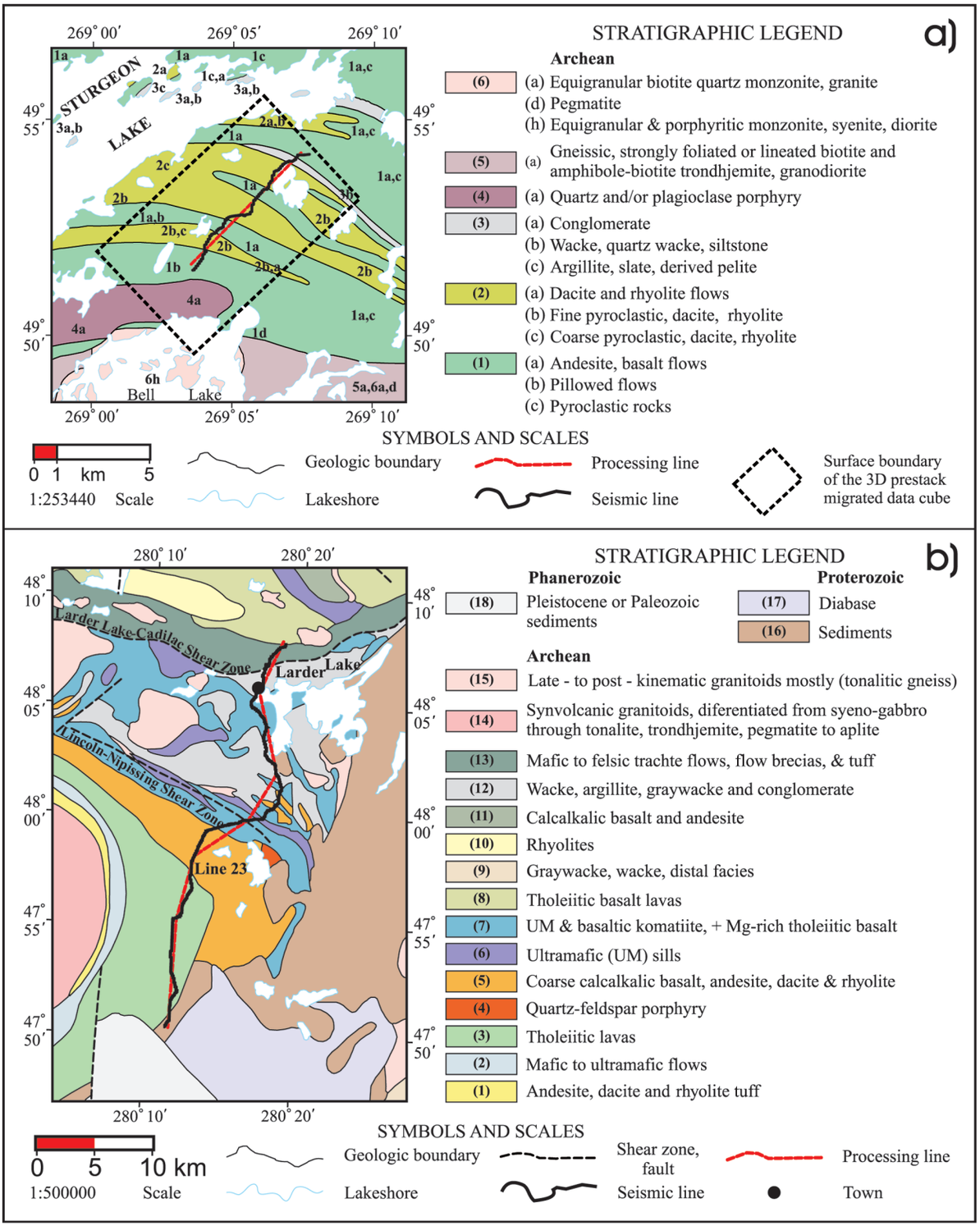

FIG. 1. Acquisition and processing geometries and the geological environments of the two surveys studied. (a) Sturgeon Lake line [based on OGS map 2442 (1980)]. (b) Lithoprobe Abitibi line 23 [based on MERQ-OGS map (1984)].

reflector geometry;

$$p_y = \frac{-2\sin\theta_y\cos\theta_x}{V_{\rm rms}\left(1-\sin^2\theta_x\sin^2\theta_y\right)^{\frac{1}{2}}}, \qquad (3)$$

where θ_x and θ_y are reflector dip components along the processing line and orthogonal to it, respectively.

The full form of p is given in Appendix C. For our purposes, when the angle between the source–receiver azimuth and the processing line azimuth for most data traces falls within the range of about ±10–20 degrees it simplifies to $p = \cos\theta_x / V_{\rm rms}$.

Equation (2) is just a version of the standard DMO equation in which an extra term—the zero-offset time anomaly from reflector cross-dip—has been added to the zero-offset traveltime. The difficulty in using it lies in the fact that p_y is unknown and dependent on the geology. It must be determined from the survey data and may be different for every reflection event. However, once p_y has been obtained, correction of the cross-line dip time anomaly should (with some caveats) be straightforward and not affect the use of standard DMO processing methods.

Solutions to focusing problems

Time anomalies arising from reflector cross-dip and variations in cross-offset of the source–receiver midpoints have frequently been a research topic after the first study carried out by Larner et al. (1979). Solutions suitable to cases where the whole reflecting section or at least extensive parts of it have similar cross-dip have been proposed by, for example, Du Bois et al. (1990), Wang and West (1991), and Kim et al. (1992). However, for igneous–metamorphic geology where structures may be highly variable, we require a method in which the CDMO associated with each reflecting event can be determined separately. Furthermore, whatever procedure is applied, it should not prevent the application of DMO partial migration to the data.

In view of the above, we have adopted a processing strategy that begins after all normal stages of prestack data processing such as static correction, amplitude normalizations, deconvolution, surface wave suppression, stacking velocity analysis, and preliminary NMO correction.

First, data are binned to a processing line, CMP gathered and NMO corrected, and partially stacked to traces representing small ranges of source–receiver offset. Constant offset sections are constructed from these partially stacked traces and are coherency filtered to reduce trace-to-trace noise and irregularity. This step greatly reduces data volume and regularizes data density but requires careful decisions about the optimum size of source–receiver offset windows.

Next, DMO partial migration is applied to the constant-offset sections in the standard manner and for the required time range, but no final stack is performed. NMO corrections may be adjusted as required by later velocity analysis. Since no CDMO correction has been applied at this point, it is possible that the DMO may interpret spatial (x) variations in cross-dip time anomaly as attributable to in-line reflector dip. However, this should not be a serious drawback—certainly much less damaging than failing to correct DMO at all. Nevertheless, it suggests that the DMO correction should only be applied to early time data where it is likely to be really needed.

Finally, the cross slowness p_y is estimated for each event as a local function of CMP position (x) and zero-offset reflection time (t_0) by a semblance analysis performed in successive (x, t_0)

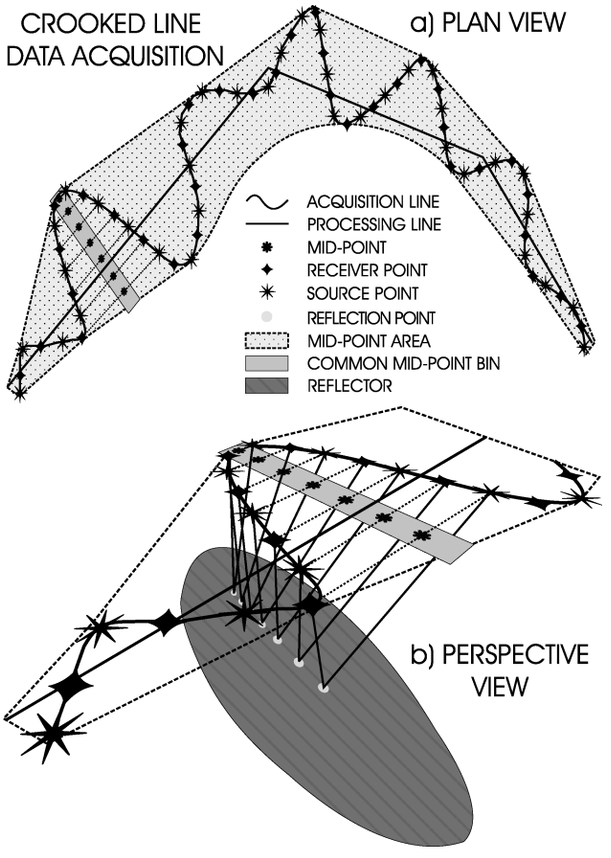

FIG. 2. A schematic of 2D crooked-line profiling. (a) A plan view. (b) A segment of (a) and a cross-line dipping reflector shown in a perspective. The crooked profile is exaggerated to better depict the data character.

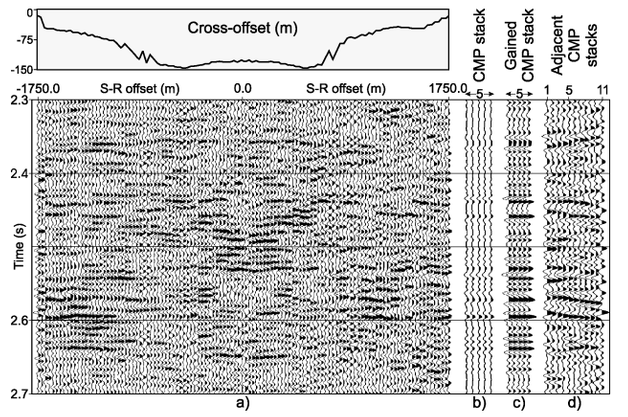

FIG. 3. Extract of NMO-corrected CMP bin gather 4555 of the Sturgeon Lake line, showing the limited and wobbly correlation of reflection events. (a) The gather, with cross-offset displayed for each trace. (b) CMP stack of (a) repeated five times. (c) Same as (b) amplified five times. (d) CMP stacks for several adjacent CMP bin gathers. The loss of signal amplitude on stacking is evident.

windows. Essentially, a suite of p_y values is chosen to cover the whole expected range of possibilities (usually several tens of values). For each p_y value a CDMO correction is computed and applied to the DMO-corrected trace set. The semblance analysis finds the p_y value that leads to optimal stacking over the whole range of source–receiver offsets in each (x, t_0) patch of the data set. An evaluation routine assesses whether a reliable p_y value has been found. For reliably determined p_y values, the data are stacked at the optimum cross-dip. Other parts of the section are obtained by standard stack at zero cross-dip.

Of course, the above strategy may not work for several reasons:

1) the shapes and layering of reflecting/scattering interfaces are so complicated that the swath 3D data do not provide enough information for it to be resolved;
2) there are too many interfering reflection events with different crossdips; and
3) the S/N ratio is too low.

If the cross-dip analysis fails, we propose a different strategy: try to apply a method of combining data traces that has a greater time (phase) tolerance than simple averaging (stacking).

In our investigations we find that a simple amplitude stack is a much more tolerant method of averaging poorly aligned signal than the standard stack. Like the cross-dip processing, amplitude processing is not a novel idea. In most other circumstances where waves are used to probe structures remotely (i.e., optical imaging, sonar, radar, etc.), the dominant wavelength in the probe wavefield is very short in comparison to the distance the waves must travel and the size of the objects being probed. Then, phase-coherent specular reflection is not the key reflection process. In these methodologies, the scalar amplitude of the reflected signal (or similar quantity such as envelope amplitude or energy) is most commonly used as the measure of reflected signal strength. It is therefore worthwhile to study how we might implement amplitude-based processing in seismic reflection imaging.

In the following sections, we first describe our methods for partial stack, local CDMO removal, and amplitude stack. Then we apply the methods to synthetic and field data. Finally, we present and discuss the results.

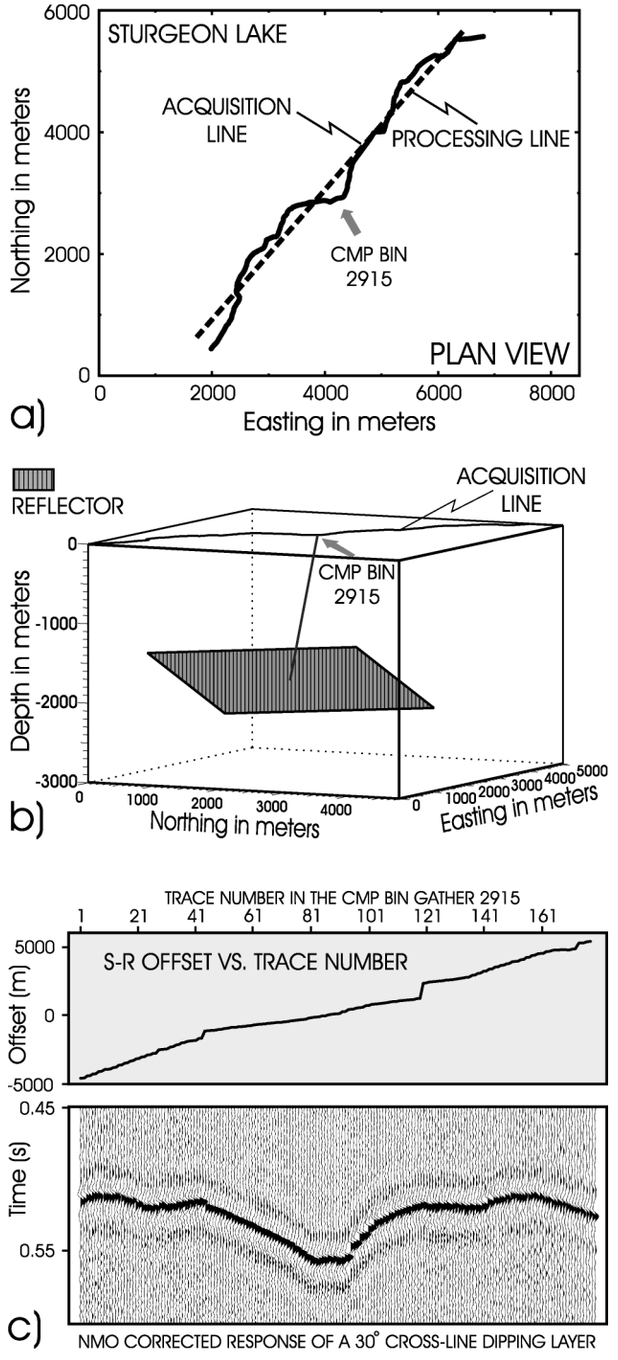

FIG. 4. Computed reflection from model A cross-line dipping sheet in one CMP bin gather of a crooked-line survey. (a) The Sturgeon Lake line geometry. (b) The 30° cross-line dipping reflector. (c) Event in CMP bin gather 2915.

METHODOLOGY

Partial stack of data

Partial stacking of an NMO-corrected CMP bin gather into a fewer number of traces representing a set of offset windows is straightforward in principle. It requires only definition of the desired offset ranges and insertion of average offset and position values into the headers of the resulting traces. When the succeeding imaging steps operate on constant offset data sections, as in DMO partial migration, partial stacking is a very useful process. It can prevent a lot of unnecessary computation and greatly increase the S/N ratio and data continuity in the constant offset gathers.

There are, however, two important challenges to overcome. First is the obvious difficulty in deciding what window size leads to an optimum result. Second, and more subtle, are problems in optimal amplitude balancing that arise when a partial stack is used to regularize data density.

Optimizing the offset window.—The goal here is to determine the maximum offset window for which partial stacking of DMO and CDMO uncorrected data still improves S/N ratio

for most of the reflection events. Nedimović and West (1999) show that cumulative stacking of data in CMP bin gathers can be used successfully to calculate the optimum offset range for partial stack. However, a more accurate and pragmatic solution is to provide quantitative statistical information on which to base the offset window selection for each data set. To do so we (a) select a representative set of NMO-corrected CMP bin gathers for the line; (b) divide the full source–receiver offset range into sets of offset windows, where the windows vary in size; and (c) compute semblance for all partial stack windows and follow this by calculating a kind of average semblance trace for the whole gather. For each test CMP bin gather, this provides a map of average semblance as a function of traveltime and offset window size. These maps make it comparatively easy to determine visually the width of the offset window at which semblance of strong events in the gather begins to fall off more rapidly with increasing offset window size than the semblance values of background noise. On this basis, offset windows of 250 and 500 m were selected for Sturgeon Lake line and Abitibi line 23, respectively, in the studies reported here.

Amplitude weighting.—When partial stacking is applied to CMP bin data from a typical crooked-line survey, one often finds the number of traces present in each of the chosen offset windows to be highly variable, from zero or one up to many tens. Furthermore, the S/N ratio of individual traces is fairly low and variable. This means that the S/N ratio of the partially stacked traces may also be highly variable. Thus, in the successor processes where each partially stacked trace will be treated equally, there is a possibility of burying very good data under some relatively large noise.

Our experience has shown the above to be an important problem, and we have found it advisable to apply amplitude weighting to the partially stacked traces that reflects an estimate of their validity or S/N ratio. The simplest method we used was to apply a weight proportional to a root power of the number of traces from which the partially stacked trace was derived. A power of about 0.5 was optimum. This weighting was used for small numbers of traces. For larger folds, a semblance trace was calculated and used in combination with the number of traces as a weighting factor.

Locally optimum cross-dip stack

After partial stacking, constant offset gathers are formed (and perhaps spatially filtered), DMO partial migration is applied using a standard method such as the log time stretch algorithm, and the result for each offset may be lightly coherency filtered to locally balance amplitudes. Then, in preparation for the CDMO analysis, the traces are sorted back to the partially stacked CMP bin gathers.

Next, a list of 20 to 100 equispaced values of cross slowness p_y is created covering the full range of possible slownesses $\pm(2/_{\min} V_{\text{rms}})$. The typical range in crystalline terrains is $\sim \pm 0.3$ ms/m. For each p_y and for all partially stacked traces in CMP bin gathers, the CDMO time shift $p_y y_i$ (where y_i is the cross-line offset of the ith trace) is calculated and applied while stacking. Thus, the equation for the cross-dip-corrected stacked trace C is the slant stack equation:

$$C(x, t_0, p_y) = \frac{1}{N(x, t_0, p_y)} \sum_{i=1}^{N} D_i(x, t), \qquad (4)$$

in which $t = t_0 + p_y y_i$ and D_i are the partially stacked trace data. Note that the number of nonzero data samples (N) selected for averaging from the partially stacked CMP volume $D_i(x, t)$ may vary with x, t_0, and p_y because of data availability and muting.

To assist in deciding the optimum p_y for each x and t_0 in the stacked section, we also compute a local running average of the stacked trace scalar amplitude (A) over $L + 1$ time samples Δt_0,

$$A(x, t_0, p_y) = \frac{1}{L+1} \sum_{l=-L/2}^{L/2} |C(x, t_0 + l\Delta t_0, p_y)|, \qquad (5)$$

as well as semblance S (Neidell and Taner, 1971) of the traces used in equation (4) for each p_y,

$$S(x, t_0, p_y) = \frac{1}{L+1} \sum_{l=-L/2}^{L/2} \left[\frac{\left[\sum_{i=1}^{N} D_i(x, t') \right]^2}{N(x, t_0, p) D_i^2(x, t')} \right], \qquad (6)$$

in which $t' = t_0 + l\Delta t_0 + p_y y_i$. The rest of the notation is the same as in equation (4).

We then combine equations (5) and (6) to form the objective function M,

$$M(x, t_0, p_y) = A(x, t_0, p_y) S(x, t_0, p_y), \qquad (7)$$

which is searched at every (x, t_0) to find the p_y value which maximizes it in a small sliding time window around t_0. In this way a new data array, called the optimum cross slowness map ${}_{opt}p_y(x, t_0)$, is obtained in preliminary form. A 1D median filter is applied to it to remove spurious events.

The reliability of the optimum cross-slowness values determined in the preliminary map may fluctuate greatly over the section, e.g., because the signal level varies greatly. A map of reliability is therefore required, and there are many possible approaches to making it. We produce a patchy binary map of reliability from an estimate of reflection absolute amplitude made by the amplitude stacking method described in the next section. The amplitude stack is converted into a binary reliability map by thresholding the stack's absolute amplitude at an experimentally determined level and then applying a 2D median filter to eliminate small anomalous regions. The preliminary map of optimum cross-slowness is multiplied on a point-by-point basis with the binary reliability map, and final estimates of optimum cross-slowness are obtained by applying a modal filter to the reliability-thresholded slowness map. If the number of points in the rectangular filter area falls below a set threshold, a value (e.g., 1E-06) indicating no determination of cross-dip is assigned. A small extension of the reliably determined cross-slownesses over the background area after the 2D mode filtering is also helpful.

The final map of optimum cross-slowness can be displayed as a color map, and it allows creation of the locally optimum cross-dip stack by a version of equation (4) in which

$t = t_0 + {}_{opt}p_y(x, t_0)y_i$. For the regions of a section where cross-slowness values were not reliably determined and an arbitrary value was assigned, the data are usually stacked at zero cross-slowness.

All data examined in this paper, synthetic and field, were processed using cross-slowness bounds ($\pm 0.\dot{3}$ ms/m) set so that all possible cross-dips ($\pm 90^\circ$) were tested for. The host medium velocities were always $\geq$6000 m/s.

Amplitude stack

Despite all efforts, CDMO analysis may not succeed. It might be necessary then to opt for the use of other imaging methods that are more tolerant to combining poorly aligned trace signals than the standard stack. Various types of amplitude processing, for example, offer several solutions to the imaging problem.

It is straightforward to convert seismic trace recordings $s(t)$ to scalar amplitude $|s(t)|$, energy $s^2(t)$, or envelope amplitude $(s^2(t) + \{H[s(t)]\}^2)^{1/2}$, where H denotes the Hilbert transform. These time series are all positive, and reflection signals are then identifiable only as local increases or fluctuations in the amplitude relative to some comparatively steady background level that can be considered noise. The tests we have done show that a simple way to extract these local changes from the steady noise background is to apply a bandpass frequency filter to the amplitude data, with the low cut point set at 0 Hz.

In our investigation of time (or phase) tolerant stacking methods, we have used trace scalar amplitude $a(t)$, which is related to the usual seismic trace by

$$a(t) = |s(t)|^P, \quad \text{where} \quad 1 \leq P \leq 2. \tag{8}$$

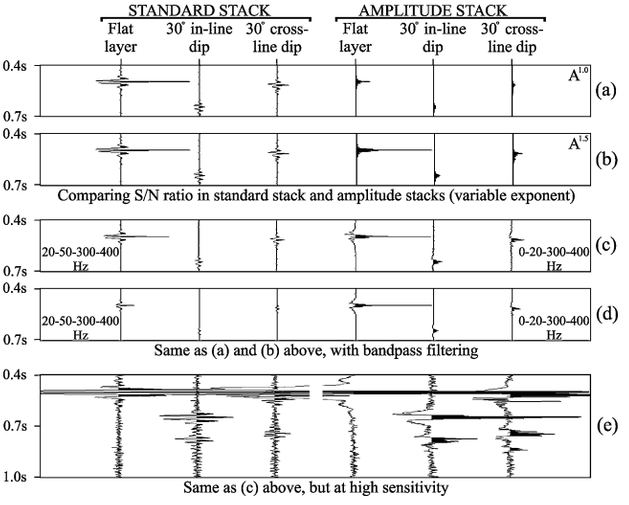

FIG. 5. Comparison of standard stacks (traces 1–3) with amplitude stacks (traces 4–6) of partially stacked synthetic data from horizontal, 30° in-line dipping and 30° cross-line dipping reflector. Within each part of the figure, the stacked traces were balanced so the random noise exhibits the same energy level. This can be seen at late times in part (e), which is identical to part (c) except for the boosted amplitude levels. The standard stacks for parts (a) and (b) are the same. The amplitude stack changes as the absolute amplitudes are raised to the power of (a) 1 and (b) 1.5.

With this measure, a constant-amplitude sine wave $s(t)$ converts to a constant level and some higher frequency—even harmonics. Random uncorrelated noise in the interval $(-1, +1)$ converts to random noise in $(0, +1)$ with different statistics, i.e., has a mean value of 0.5 and half the standard deviation of the original. There may appear to be some value in using the envelope amplitude $(s^2(t) + \{H[s(t)]\}^2)^{1/2}$ instead, as the high-frequency components would be reduced. However, our experiments have shown no benefits commensurate with the

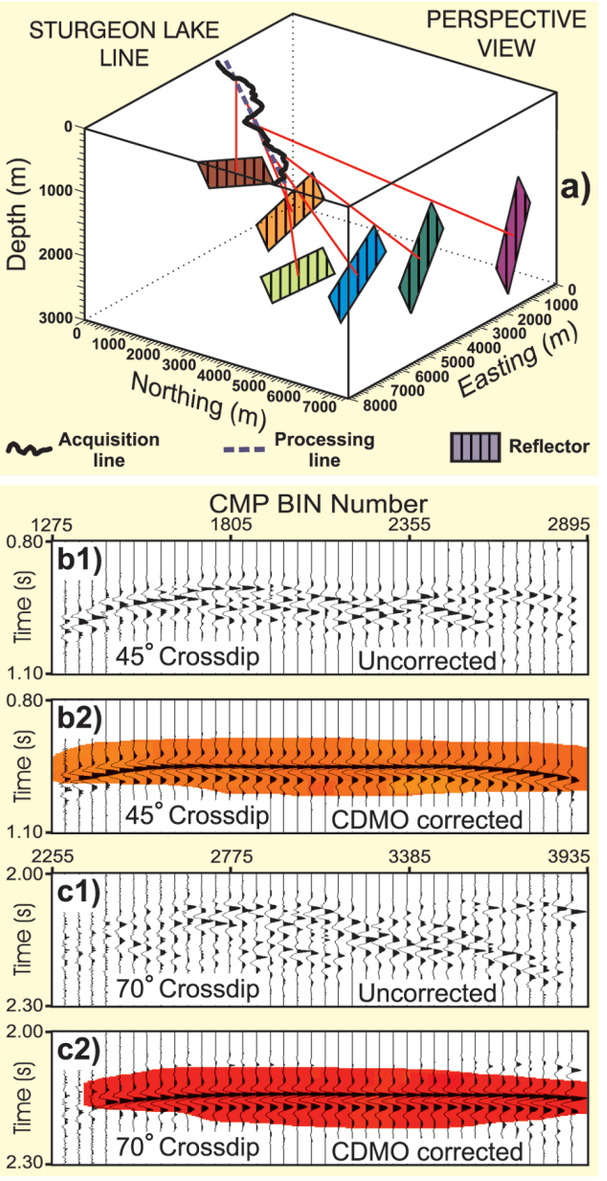

FIG. 6. (a) Model B includes six reflectors that dip toward the acquisition/processing line (~SE). Reflectors are squares with 1500-m sides and true dips of 0°, 15°, 30°, 45°, 60° and 70°. Tops are all positioned at a depth of 1500 m. Source signal is a 20–300-Hz Butterworth minimum-phase wavelet. Parts (b1) and (c1) of the section illustrate the standard stack of the 45° and 70° dipping events, respectively. The corresponding locally optimum cross-dip stacks are shown in parts (b2) and (c2).

additional computation cost, and even some unnecessary loss of resolution.

Producing amplitude stacks is a fairly simple procedure. Processing continues in a standard fashion to the point where the partially stacked, NMO- and DMO-corrected and coherency-filtered trace data would ordinarily be stacked into traces of the SZOST section. At this point, the traces in the CMP bin gathers are converted to amplitudes $a(t)$. They are then stacked in the usual way. A bandpass filter is applied before and/or after the stacking to at least remove the slowly varying noise background from the all-positive traces. To further optimize it, the amplitude stack is coherency filtered.

As an illustration of the efficiency of amplitude stacking, we have applied it to a number of model responses: a horizontal layer, a 30° in-line dipping reflector, and a 30° cross-line dipping reflecting sheet. Figure 4 shows the 30° cross-line dipping reflector and the crooked-line acquisition geometry (model A) as well as the synthetic data from CMP bin gather 2915. The models for the horizontal and the 30° in-line dipping reflector are identical except for the different orientation of the reflector. Data in CMP bin gather 2915 for all three models was NMO corrected and partially stacked using a 200-m offset window. Signal from both dipping events in the partially stacked traces shows severe time alignment problems. For the 30° cross-line and the 30° in-line dipping event, the arrival times of the partially stacked signals differ up to 50 and 15 ms, respectively, whereas the signal wavelet is a 20–300 Hz Butterworth minimum-phase wavelet with ~5 ms half-cycle width.

The test results obtained on all three models by standard and amplitude stacking of the partially stacked synthetic data from CMP bin gather 2915 are shown in Figure 5. Because modeled data traces before stack all contain the same amount of random noise in the entire time interval (0–2 s) and no reflection/diffraction signals occur beyond 0.9 s, it was possible to scale stacked trace amplitudes within each panel of Figure 5 so they also exhibit the same noise levels (observe the amplitudes at late times in Figure 5e). This does not alter the relative amplitudes within any of the trace groups but shows how standard and amplitude stacking affect S/N ratio.

Figures 5a–d all show that when the signal cannot be aligned well for averaging because reflectors are dipping, the obtained stacked trace will show very weak and diffuse events compared to the stacked trace of a horizontal reflector. But when compared with standard stacks, the amplitude stacks of poorly aligned signal in all cases show better focusing and, after the bandpass filter, about twice better S/N ratio. The effect of changing the exponent in amplitude stacking is also evident in Figure 5. But although raising the exponent raises the S/N

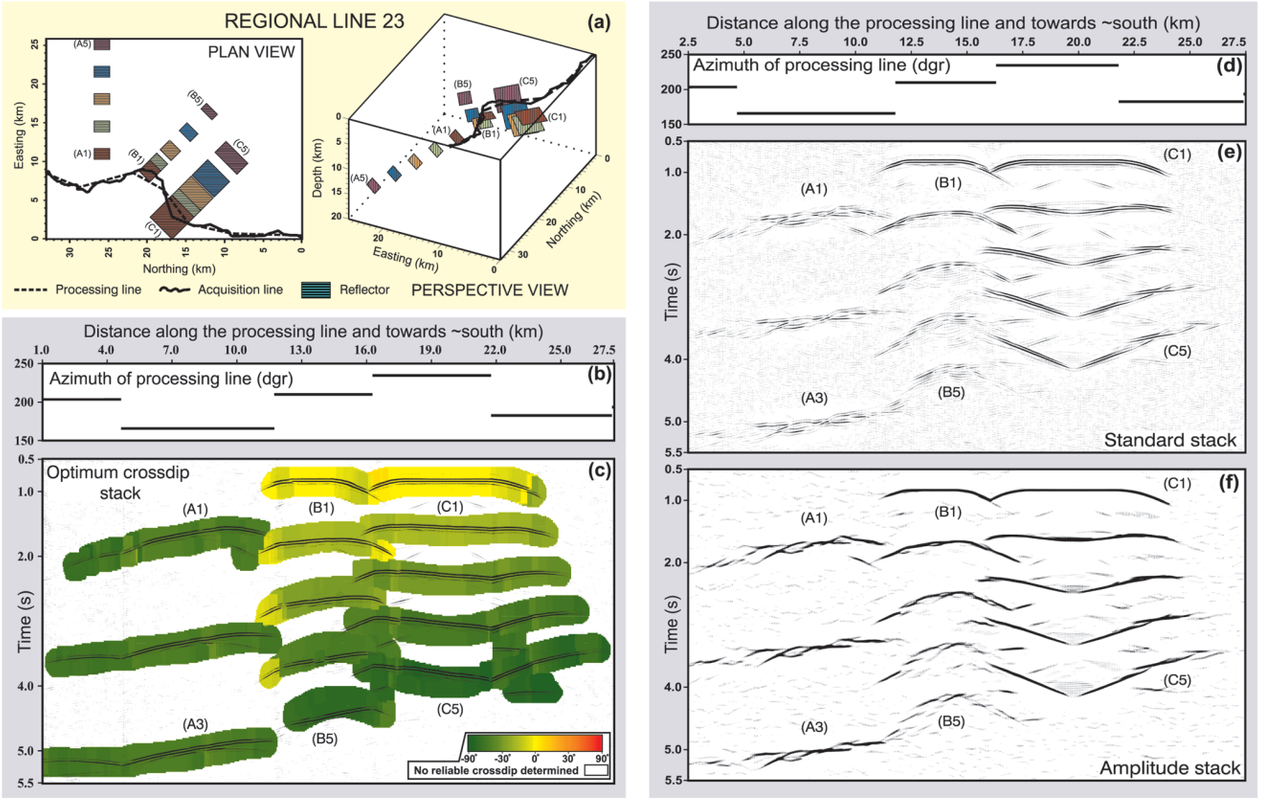

FIG. 7. (a) Model C: Line 23 acquisition geometry and three groups of five reflectors. The most northerly group (A) has five reflectors predominantly dipping in the cross-line direction at 45° true dip. The sheets in groups B and C are positioned to reflect energy toward the middle segment of the acquisition line, where their events will partially overlap in the time section. Dips in groups B and C are 0°, 15°, 30°, 45°, and 60°. All except the horizontal reflectors exhibit both in-line and cross-line components of dip. (c) The locally optimum cross-dip stack includes all but the two deepest events from group A. (e, f) The corresponding parts of the standard stack and the amplitude stack, respectively. (b, d) Azimuth of the processing line.

ratio of the amplitude stacks considerably, both with and without filtering, it also increases the contrast between the three events because it heavily favors large amplitudes. Therefore, an exponent value as large as two may be undesirable.

Our experience shows that the overall best amplitude sections are obtained by using an exponent of ~1.5. However, for some specific goals such as imaging the Moho discontinuity, using an exponent of 2 and not balancing the amplitudes nor filtering the data after the stack may improve the image.

RESULTS ON MODELED DATA

Model B (Figure 6a) was specifically designed to investigate CDMO and test the procedures designed to remove it. Figures 6b and 6c show the selected results: standard and cross-dip stack of 45° and 70° dipping events. Events on the standard stack (b1 and c1 in Figure 6) appear as numerous, short, in-line dipping reflectors. After the locally optimum cross-dip stack (b2 and c2 in Figure 6), the reflections are well focused and S/N ratio is dramatically improved. All events have the same expression as they would if the acquisition had been done along the processing line; they become interpretable on a 2D seismic profile. In addition, the cross-dip of the reflectors (see the cross-dip color palette in Figure 7c) is determined and superimposed on the stacked image as colored background to aid interpretation. Clearly, the imaging techniques we have designed have done a good job.

A side effect of the cross-dip problem is its effect on velocity analysis. Regardless of the method used, no truly meaningful result could be obtained from model B synthetic data. The results of CDMO processing shown in Figure 6 were computed by using the known host medium velocity of the model. Indeed, the magnitude of CDMO is so large for model B data, even though the average cross-offset aperture of the Sturgeon Lake line geometry is small (~350 m), that it reaches well over 100 ms for the 45° dipping event and more than 200 ms for the 70° dipping event.

Even when dealing with data acquired in crystalline terrains where the velocities at large scale usually change only gradually and uniformly and in structures with less extreme cross-dip than in model B, CDMO effects can complicate velocity analysis. It is advisable, therefore, to choose the data used for velocity analysis carefully to have minimum variation in cross-offset. We also suggest a simple procedure for extracting an improved velocity model. Just as is done with NMO and DMO where velocity analysis is repeated after the DMO correction, for crooked-line data from crystalline terrains velocity analysis can be redone after an initial CDMO correction; then the NMO, DMO and CDMO can be revised.

Line 23 has a very crooked, multiple-segment processing line. However, it has a relatively shorter spread compared to reflector depth than the Sturgeon Lake line. To further test our CDMO imaging procedures, we computed a synthetic data set by using the geometry of this crustal-scale seismic survey,

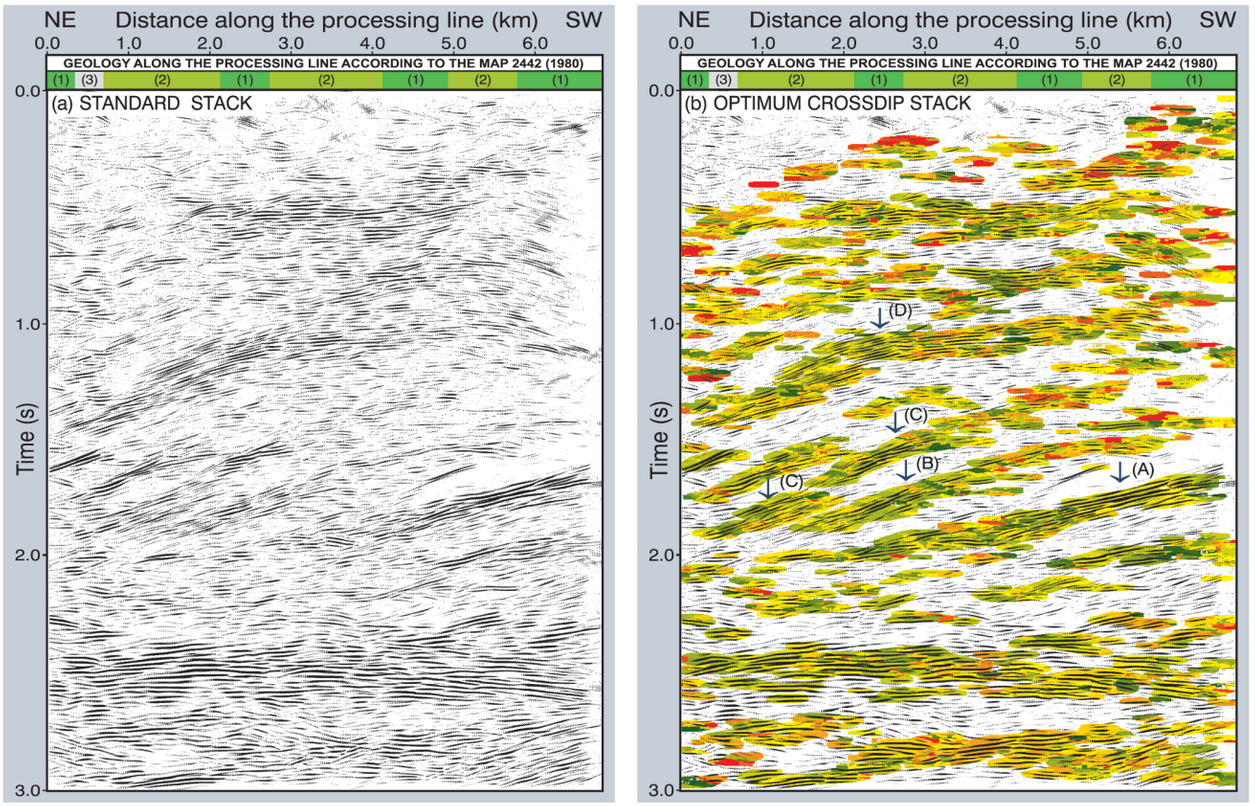

FIG. 8. Standard stack (a) and locally optimum cross-dip stack (b) of the Sturgeon Lake line data. The cross-dip color palette for the extracted cross-dip color map underlying the locally optimum cross-dip stack is given in Figure 7c.

reflectors of model C (Figure 7a), and a 10–56 Hz Klauder wavelet.

Figure 7 shows the locally optimum crossdip stack (c), standard stack (e), and amplitude stack (f) together with the processing-line azimuth (b, d) of model C data. The reflectors in the optimum cross-dip stack are continuous along the straight segments of the processing line. As expected, the only breaks occur where the slalom line changes direction. Signal focusing and S/N ratio are far better than for the corresponding standard and amplitude stacks. The obtained cross-dip stack, when superimposed on a cross-dip color map, provides the necessary information for a meaningful interpretation. Because NMO, DMO, and CDMO are all present in model C data, the results show that all three moveouts can individually be corrected for successfully and an accurate image of the subsurface structures obtained. But this can be achieved only when the processing line is kept straight and is composed of as few segments as possible. Furthermore, straight-line sections facilitate interpretation and are essential if the processed sections are to undergo 2D migration.

Several other important observations were made. First, events corresponding to the A and B groups of reflectors spread greatly apart from each other in space as their distance from the acquisition/processing line increases. This structural information cannot be inferred from the standard stack but can be extracted from the cross-dip stack. Second, events on the standard stack show incorrect apparent in-line dips and are defocused. Third, in the standard stack, reflectors show breaks where the processing line is straight but where the acquisition line experiences an abrupt change in direction, even if there is defocusing from CDMO. Fourth, reflectors of group C have a stronger signal on the standard stack than those of the other two groups. The main reason for their better focusing is a relatively straighter acquisition line in the region where these reflectors direct the energy back to the acquisition/processing line. Finally, predominantly cross-line dipping reflectors of group A exhibit a very similar signature on a standard stack, experimentally confirming that CDMO is not a function of depth/time.

When the CDMO is present in the data, neither standard nor amplitude stack is an accurate image. However, the amplitude section, though exhibiting the same problems as a standard section, shows a higher signal focusing and a better S/N ratio.

RESULTS ON FIELD DATA

Sturgeon Lake line.—The standard stack and the optimum cross-dip stack of the field data are shown in Figure 8. The striking feature on both sections is the nearly omnipresent reflectivity. According to the optimum cross-dip stack, most of the observed reflections come from reflectors that appear to be dipping toward the north. This means most of the imaged reflectors lie southeast of the acquisition/processing line. While the observed reflectivity is pervasive, it differs in strength and character along the profile and even more so with depth. The strongest events are recorded at late times (1.5–3.0 s). The deepest are subhorizontal and could outline the top of a basement upon which the greenstones were erupted—possibly a large batholith or a massive gneissic domain intruded by many subhorizontal sills. The greenstones appear to be intruded and pushed aside by younger intrusive rocks of units 4, 5, and 6 (see Figure 1a). Groups of reflectors thought to be related to these intrusive rocks are indicated in Figure 8b as A, B, C, and D. These have strong components of both in-line and cross-line dip and appear to be the steepest events in the section. Reflections that are shallower than ~1 s are believed to be caused by the varying lithology within the greenstones of the Sturgeon Lake belt. The maximum depth of the greenstones is estimated at ~3 km. Although many shallow events are visible, no direct correlation between them and the surface geology can be made.

Abitibi line 23.—The CDMO analysis of this data provided only a small amount of reliable cross-dip information, not enough to provide a useful CDMO stacked section. Therefore, we compare line 23 standard stack (Figure 9a) with the corresponding amplitude stack (Figure 9b). We show the part of both sections with most of the reflection events. The amplitude stack of line 23 data, best viewed sideways and from a greater distance than the standard section, provides a better display of the general structural trends and has a better S/N ratio than the standard stack. The largest concentration of reflectivity, found at ~2 s near the north end of the line and then shallowing toward the Proterozoic sediments at the south end, may be a sheared contact between the Abitibi greenstones and the basement structure. Below it is a zone void of reflectivity which extends to ~4 s (~12 km). From 4 to 10 s is an extensive zone in the lower crust made up mostly of mildly dipping reflective events. This is commonly observed elsewhere in the crystalline crust. However, the closeness of the surface outcrop of

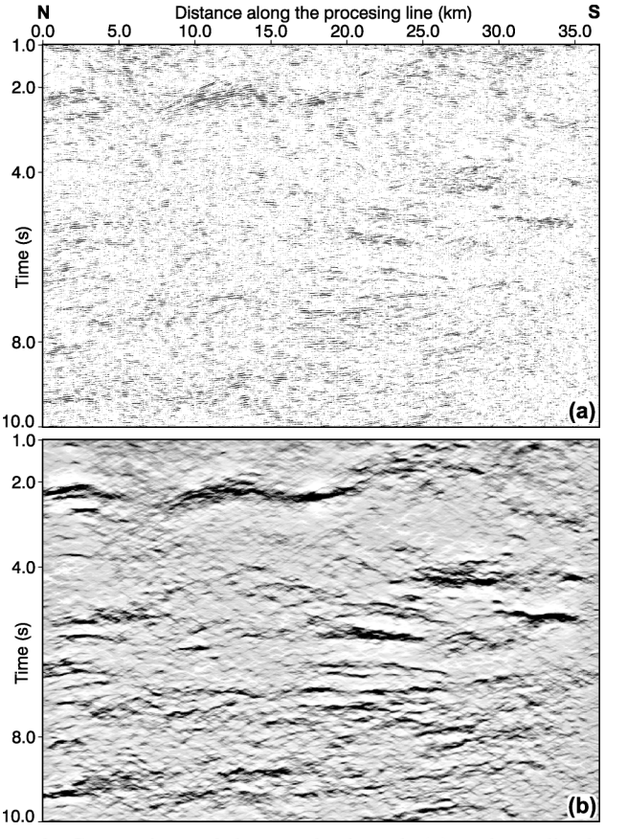

FIG. 9. Comparison of the standard stack (a) and amplitude stack (b) of the line 23 data.

Proterozoic diabase rocks (see Figure 1b) also allows for speculation that some or all of this reflectivity may be caused by sills and undulating sheets that intrude the deep crust.

CONCLUSIONS

We have described two methods for improved stacking of 2D high-fold, crooked-line seismic reflection data: the optimum cross-dip stack and the amplitude stack. The former is the preferred approach because the stack is improved by better alignment of trace signals in the CMP bin gathers. This is done by including the cross-dip terms in the traveltime equation and analyzing the reflector cross-dips. Once the reflector cross-dip is known, CDMO is removed and the data are stacked. Superposition of the cross-dip stack on the cross-dip color map provides the interpreter with precious 3D information about the imaged structures. Amplitude stacking is considered a last resort because it aims only at minimizing the damage in signal averaging when the signal in the CMP bin gathers cannot be focused before applying stacking. Nevertheless, it is very useful when the optimum cross-dip method fails to extract enough 3D information.

Both methods have their drawbacks. The optimum cross-dip method cannot extract the cross-dip of both of the events whose reflection responses overlap on the section. Only the stronger event remains in the stack. The amplitude stack, although it yields a section with improved S/N ratio, is as inaccurate an image as the standard stack. But in spite of their limitations, the results obtained on synthetic and field data show that both methods produce a better section than the standard stack. We suggest that they be used in routine processing of 2D crooked-line data.

ACKNOWLEDGMENTS

This research was part of M. R. N.'s Ph.D. thesis project and was supported in part by funding for G. F. W. from the Natural Sciences and Engineering Research Council of Canada. Early progress on cross-dip processing by Weizhong Wang when he was a research fellow at the University of Toronto served as a foundation for the work. We are very thankful to Larry Petrie and Larry Matthews of Noranda Mining and Exploration Inc. for providing Sturgeon Lake line data. Abitibi line 23 data were kindly provided by Project Lithoprobe. M. R. N. expresses his gratitude to Dr. Roy Hyndman of the Geological Survey of Canada—Pacific for his support during the preparation of this manuscript. We are also grateful to Carlos Calderón and Reinaldo Michelena for their constructive reviews of the manuscript.

REFERENCES

Du Bois, L., Levato, L., Escher, A., Marchant, R., Oliver, R., Ouwehand, M., Sellami, S., Steck, A., and Wagner, J. J., 1990, Pseudo-3D study using crooked line processing from the Swiss Alpine western profile–Line 2 (Val dÁnniviers-Valais): Tectonophysics, **173**, 31–42.

Kim J., Moon, W. M., Percival, J. A., and West, G. F., 1992, Seismic imaging of shallow reflectors in the eastern Kapuskasing structural zone, with correction of cross-dip attitudes: Geophys. Res. Lett., **19**, 2035–2038.

Larner, K. L., Gibson, B., Chambers, R., and Wiggins, R. A., 1979, Simultaneous estimation of residual statics and crossdip time corrections: Geophysics, **44**, 1175–1192.

MERQ-OGS, 1984, Lithostratigraphic map of the Abitibi subprovince: Ontario Geological Survey/Ministré de l'Énergie et des Ressources, Québec, catalogued as Map 2824 in Ontario and DV 83-16 in Québec, scale 1:500 000.

Nedimović, M. R., and West, G. F., 1999, Processing seismic reflection data from high fold, crooked line surveys in crystalline geological terrain: 69th Ann. Internat. Mtg., Soc. Expl. Geophys., Expanded Abstracts, 1437–1440.

——— 2003, Crooked-line 2D seismic reflection imaging in crystalline terrains: Part 2, migration: Geophysics, **68**, 286–296, this issue.

Neidell, S. N., and Taner, T. M., 1971, Semblance and other coherency measures for multichannel data: Geophysics, **36**, 482–497.

OGS, 1980, Sioux Lookout-Armstrong map 2442, *in* Geological compilation series, Kenora and Thunderbay districts: Ontario Geological Survey, Ministry of Natural Resources, scale 1:253 440.

Wang, W., and West, G. F., 1991, Stacking processes of crooked lines using the SUN/INSIGHT System: Lithoprobe Seismic Processing Facility Newsletter, **4**, 13–18.

APPENDIX A

DETAILS ABOUT FIELD DATA

The Sturgeon Lake line data were collected by using a 7.84-km-long fixed spread with 393 active receiver groups spaced every 20 m. These recorded each of 182 shots spaced at 40-m intervals for 3 s. Small explosive charges (0.5 kg) in holes drilled to bedrock were the sources of energy. The recorded signal has a wide bandwidth ranging from several to more than 300 Hz.

Lithoprobe's Abitibi line 23 crustal scale profile is 41.4 km long. The data were gathered by using a 12-km spread with 240 receiver groups spaced at 50 m. Listening time was 18 s. The energy source was a group of four vibrators operated eight times to cover an interval of 100 m around each of the 403 source points. Source signal was a linear upsweep with a frequency range from 10 to 56 Hz.

For both surveys, the CMP bin interval chosen for data processing is the same as the corresponding receiver group interval. The bin height was chosen to include all data.

APPENDIX B

MODELING METHOD

The ray-Born method was used with a constant compressional wave velocity (6 km/s) assigned to the host medium. In this method, reflectors are represented by a dense grid of point scatterers approximating a continuous sheet. Although it can handle curved reflectors, only planar reflectors were studied. The effect of a thin, low-velocity layer (1.5 km/s) on raypath geometry and amplitudes was taken into account. Vertical displacement at the free surface was calculated neglecting any reverberation. Directivity of the vibrator source was accounted for by a cosine function. A Butterworth minimum-phase wavelet (20–300 Hz) was used to compute synthetic data for models with the Sturgeon Lake line geometry. A Klauder wavelet (10–56 Hz) was used to compute synthetic data for models that use the Lithoprobe–Abitibi line 23 geometry. Gaussian random noise was added to all synthetic data produced.

APPENDIX C

CROSSDIP MOVEOUT (CDMO)

For any planar reflector in a uniform host medium of velocity V, the source–reflector–receiver traveltime (t) observed in a trace whose midpoint is displaced from the processing line can be expressed as

$$t^2(x, y, h) = (t_0(x) + p_y y)^2 + p^2 h^2, \tag{C-1}$$

where t_0 is the zero-offset traveltime, h is the total source–receiver distance with component $x = h\cos\varphi$ along the processing line, y is the cross-line offset, and $p_y y$ is called the crossdip moveout (CDMO). The slowness terms p and p_y are dependent on the source–receiver azimuth (φ), reflector dip component along the processing line (θ_x), reflector dip component orthogonal to the processing line (θ_y), and velocity (V) of the host medium (see Figure C-1). In terms of the model parameters,

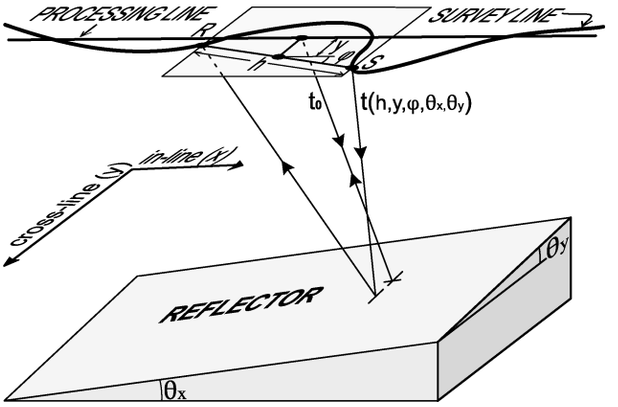

FIG. C-1. An example of a raypath in 2D crooked-line surveying. The terms S and R are source and receiver, respectively.

$$p = \left[\frac{1 - \sin^2\theta_x + \sin^2\varphi\left(\sin^2\theta_x - \sin^2\theta_y\right) + \frac{1}{4}\sin 2\varphi \sin 2\theta_x \sin 2\theta_y}{V^2\left(1 - \sin^2\theta_x \sin^2\theta_y\right)}\right]^{\frac{1}{2}} \tag{C-2}$$

and

$$p_y = \frac{-2\sin\theta_y \cos\theta_x}{V\left(1 - \sin^2\theta_x \sin^2\theta_y\right)^{\frac{1}{2}}}. \tag{C-3}$$

When $\sin^2\varphi \ll 1$ or when $h \ll h_{\max}$ and $\sin^2\theta_x \sin^2\theta_y \ll 1$, p may be adequately approximated as

$$p = \left[\frac{1}{V^2} - \frac{\sin^2\theta_x}{V^2}\right]^{\frac{1}{2}} = \frac{\cos\theta_x}{V}, \tag{C-4}$$

which is the usual DMO equation. In practice, when processing seismic data, p and p_y must be extracted from the data themselves. Usually, p is estimated by moveout analysis as a smooth function of t_0 and x and is interpreted as $1/V_{\text{rms}}$ or $\cos\theta_x / V_{\text{rms}}$, where V_{rms} is the root mean square velocity.